4-20-1998

White Dwarf Cosmochronometry. I. Monte Carlo Simulations of Proper-Motion- and Magnitude-Limited Samples Using Schmidt's 1/Vmax Estimator

Matt A. Wood
Florida Institute of Technology, wood@kepler.pss.fit.edu

Terry D. Oswalt
Florida Institute of Technology, oswaltt1@erau.edu

THE ASTROPHYSICAL JOURNAL, 497:870–882, 1998 April 20

WHITE DWARF COSMOCHRONOMETRY. I. MONTE CARLO SIMULATIONS OF PROPER-MOTION– AND MAGNITUDE-LIMITED SAMPLES USING SCHMIDT'S $1/V_{\max}$ ESTIMATOR

MATT A. WOOD AND TERRY D. OSWALT
Department of Physics and Space Sciences, Florida Institute of Technology, Melbourne, FL 32901-6988; wood@kepler.pss.fit.edu, oswalt@tycho.pss.fit.edu
Received 1997 February 14; accepted 1997 June 24

ABSTRACT

Observationally, white dwarf stars are a remarkably homogeneous class with a minimum observed $T_{\rm eff} \sim 4000$ K. Theoretically, the physics that determines their cooling timescales is relatively more straightforward than that which determines main-sequence evolutionary timescales. As a result, the white dwarf luminosity function has for the last decade been used as a probe of the age and star formation rate of the Galactic disk, providing an estimated local disk age of ~ 10 Gyr with estimated total uncertainties of roughly 20%. A long-standing criticism of the technique is that the reality of the reported downturn in the luminosity function (LF) hinges on just a handful of stars and on statistical arguments that fainter (older) objects would have been observed were they present. Indeed, the likely statistical variations of these small-number samples represent one of the primary uncertainties in the derived Galactic age, and the behavior of Schmidt's $1/V_{\max}$ estimator in this limit is not well understood.

In this work, we explore these uncertainties numerically by means of a Monte Carlo population synthesis code that simulates the kinematics and relative numbers of cooling white dwarfs. The "observationally selected" subsamples are drawn using typical proper motion and V-magnitude limits. The corresponding $1/V_{\max}$ LFs are then computed and compared to the input-integrated LFs. The results from our (noise-free) data suggest that (1) Schmidt's $1/V_{\max}$ technique is a reliable and well-behaved estimator of the true space density with typical uncertainties of $\sim 50\%$ for 50 point samples and 25% for 200 point samples; (2) the age uncertainties quoted in previously published observational studies of the LF are consistent with uncertainties in the Monte Carlo results—specifically, there is a $\sim 15\%$ and $\lesssim 10\%$ observational uncertainty in the ages inferred from 50 point and 200 point samples, respectively; and (3) the large statistical variations in the bright end of these LFs—even in the large-N limit—preclude using the white dwarf LF to obtain an estimate of the recent star formation rate as a function of time.

Subject headings: methods: statistical — stars: luminosity function, mass function — stars: statistics — white dwarfs

1. INTRODUCTION

The use of white dwarf (WD) stars as a probe of the Galactic age has a long history, dating to Schmidt's (1959) realization that the Mestel (1952) cooling law could be used to provide a lower limit to the age of the Galaxy if a downturn in the white dwarf luminosity function (WDLF) could be observationally detected—i.e., if a *lack* of white dwarfs fainter than some luminosity were discovered and could be shown to be statistically significant (see also D'Antona & Mazzitelli 1978 and the review by Koester & Chanmugam 1990). Winget et al. (1987) compared theoretical WDLFs to the preliminary observational results of Liebert and collaborators that showed a downturn at a luminosity of $\log (L/L_{\odot}) \approx -4.4$. These authors estimated a local disk age of 9.3 Gyr and suggested a lower limit to the age of the universe of $t_{\rm univ} \gtrsim 10.3$ Gyr. Liebert, Dahn, & Monet (1988, hereafter LDM; see also Liebert, Dahn, & Monet 1989) presented a detailed analysis of their observations using the $1/V_{\max}$ method of Schmidt (1968). They concluded that the deficit of white dwarf stars cooler than $T_{\rm eff} \sim 4000$ K in their sample reflects a true paucity of faint white dwarfs and is not the result of some selection effect.

The theoretical implications of the shape of the LDM luminosity function (LF) have been studied by several authors, including Iben & Laughlin (1989), Yuan (1989, 1992), García-Berro et al. (1988), Noh & Scalo (1990), Wood (1990, 1992, 1995), and Hernanz et al. (1994). Many of these studies produced age estimates consistent with the Winget et al. (1987) results to within 1–2 Gyr—not surprising, since most used the Winget et al. or Wood (1992) C-core cooling curves. However, Wood (1995) using C/O-core, DA models with updated opacities and more realistic H/He/C/O composition profiles, found $t_{\rm disk} \approx 7.5$ Gyr when comparing with the LDM data (see also Oswalt et al. 1996). Such young age estimates for the local Galactic disk are difficult to reconcile with the $t_{\rm halo} \approx 15$ Gyr ages of the old halo globular clusters (Bolte & Hogan 1995; Chaboyer 1995) because essentially all Galactic formation and chemo-evolutionary models suggest delays of ~ 3 Gyr at most between the onset of star formation in the halo and in the local disk (e.g., Burkert, Truran, & Hensler 1992, but cf. Chiappini, Matteucci, & Gratton 1997).

We note that one proposed solution to this age problem is the phase separation model (see Segretain et al. 1994; Hernanz et al. 1994 and references therein). Within this model, the spindle form of the C-O phase diagram yields an O-rich solid with a thin overlaying C-rich fluid layer; a Rayleigh-Taylor instability mixes this fluid into the C-O fluid above. The release of binding energy (i.e., the change in gravitational plus internal energy) acts to increase the cooling timescale by 10%–20% at the luminosity of the LDM downturn. The efficiency of the phase separation process, however, is a matter of some debate within the white dwarf community. In any event, the phase separation model does not affect the conclusions of this work, since we are not attempting to derive absolute ages, and we do not discuss it further.

Recently, Oswalt et al. (1996, hereafter OSWH) published

a preliminary LF based on 50 stars observed as part of their survey of common proper-motion binaries. Their results ($t_{\rm disk} \approx 9.5^{+1.1}_{-0.8}$ Gyr but with no upper limit at the 2 σ level) indicate a downturn age roughly 2 Gyr older than that of LDM using the same (Wood 1995) models. This new estimate is formally consistent with the age of the halo globular cluster system at the 2 σ level but is difficult to reconcile with the 7.5 Gyr revised age of the LDM sample. The LDM and OSWH results are shown in Figure 1. Also shown are theoretical LFs integrated numerically using the code LFINT (see Wood 1992 and below). The LDM points and the LFINT curves have been normalized to the OSWH integrated space density to facilitate intercomparison. The OSWH space density of ~ 5 per 10^3 pc^3 is roughly a factor of 2 above the LDM-quoted value of ~ 3 per 10^3 pc^3, which raises the question: Are factor of 2 variations to be expected using the $1/V_{\rm max}$ method, and how closely do such estimated space densities predict the actual space density of the parent population?

More importantly for white dwarf cosmochronometry: How reliable are the observed LFs at the faint end where the numbers of objects in the faintest populated LF bin is $N \lesssim 3$? Are the error estimates given by LDM and OSWH reasonable? These are not trivial questions. Because of the need to establish a complete observational sample, only a few of all known white dwarfs contribute to the empirical luminosity function. Although observed disk kinematics suggest that because of radial mixing our sample represents an annulus in the Galaxy with radial extent $R \sim R_0(1 \pm \frac{1}{4})$ (e.g., Carney, Latham, & Laird 1990), it is impossible to know a priori if our observed sample happens to be statistically anomalous in some way. The uncertainties are exacerbated by the use of the $1/V_{\rm max}$ method, the noise properties of which are not well understood, particularly in the limit of small N (see Felton 1976). For example, bright objects near the sample proper-motion limit receive high weight in the $1/V_{\rm max}$ method, and so small changes in the adopted survey limits can have a large effect on the derived luminosity function (cf. Oswalt & Smith 1995 with OSWH).

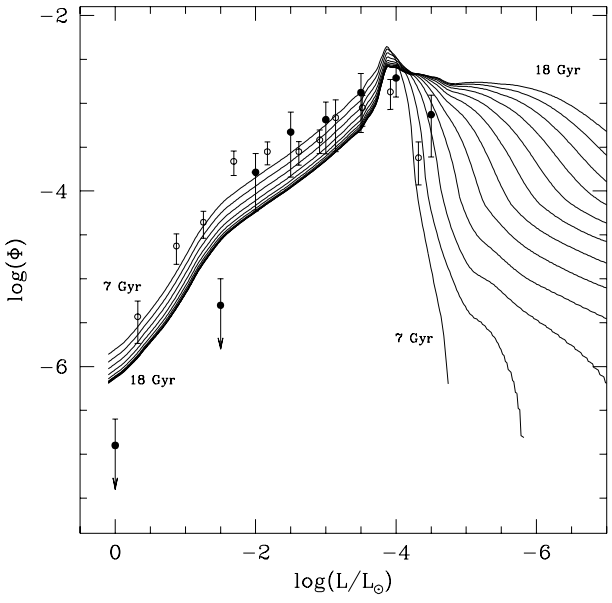

FIG. 1.—The observed LDM (*open circles*) and OSWH (*filled circles*) luminosity functions. Also shown are numerically integrated LFs using the parameters discussed in the text. The best-fit 9.5 Gyr isochrone is shown as a histogram binned as the observed data of OSWH. To facilitate comparison with the previous results, the LDM points have been vertically shifted to match the integrated OSWH space density of 0.0076 pc^{-3}. The integrated LFs have all been normalized to this cumulative density for luminosities brighter than log $(L/L_\odot) = -4.75$, the lower boundary of the OSWH LF.

To understand the behavior of the $1/V_{\rm max}$ estimator, we have explored the uncertainties in the observed luminosity function by means of extensive Monte Carlo (MC) simulations. The resulting code, MCGoLF (= Monte Carlo Generator of Luminosity Functions), populates a computational space with a pseudo-random sample whose kinematics are similar to those of the observed sample and whose relative number statistics are obtained by drawing from a probability density distribution defined by an integrated luminosity function calculated with the code LFINT (see Wood 1992). From here, the sample is culled by proper motion and limiting V apparent magnitude, as described in § 2. The objects retained in a given sample are then used to derive a $1/V_{\rm max}$ luminosity function for that sample. In § 3, by drawing a large number of independent samples and comparing these against both the observed samples and the integrated theoretical LFs, we empirically quantify the uncertainties in the derived disk ages resulting from low-N statistics at the faint end of the white dwarf luminosity function. We conclude in § 4 with an assessment of the precision inherent in the determination of the age and star formation history of the local Galactic disk from studies of the WDLF.

2. THE SIMULATION PROGRAM MCGoLF

2.1. *User Inputs*

The user inputs to MCGoLF include the number of "stars" in the final sample $N_{\rm obs}$, the disk age in billions of years $t_{\rm disk}$, the *maximum* distance (in parsecs) for the sample objects $D_{\rm max}$, the root mean squared velocity $v_{\rm rms}$ (in kilometers per second), the lower proper-motion limit $\mu_{\rm lim}$ (in arcseconds per year), the apparent V magnitude limit $V_{\rm lim}$, an evolutionary summary file from WDEC (the White Dwarf Evolutionary Code) (Lamb & Van Horn 1975; Wood 1995), an integrated theoretical LF calculated with LFINT (see Wood 1992), and the number of samples to calculate for each input parameter set $N_{\rm samp}$.

2.1.1. *Populating the Space: Theoretical Selection*

We use the following notation: $P(0, 1)$ indicates a uniform deviate between the limits 0.0 and 1.0, and $G(\sigma)$ indicates a normal (Gaussian) deviate with variance σ and zero mean. The normal deviate is calculated using the Box-Muller method (see Press et al. 1986, § 7.2). The heart of any Monte Carlo simulation code is the uniform deviate pseudo-random number generator. MCGoLF uses portable FORTRAN code developed by Marsaglia (1987). It passes all of the tests for random number generators and has a period of 2^{144}.

The algorithm at the heart of MCGoLF is quite simple. We populate a volume $V_{\rm samp}$ with $N_{\rm tot}$ objects, drawing our "observationally selected" subsample from this population. The observer is stationary at the origin of the coordinate system. Positions are assigned by three calls to the random number generator

$$x_j = P(0, D_{\rm max}) , \quad j = 1, 2, 3 , \tag{1}$$

where points are rejected if $|\boldsymbol{r}| > D_{\rm max}$, and where $D_{\rm max}$ is chosen to be well beyond the maximum distance of any object in any observationally selected subsample. Because

only the first octant is populated, the volume of the sample is $V_{\rm samp} = (\pi/6)D^3_{\rm max}$, the true space density is $\Phi_{\rm true} = N_{\rm tot}/V_{\rm samp}$, and the mass density is $\rho = \Phi_{\rm true}\langle m\rangle$, where $N_{\rm tot}$ is the *total* number of objects in the sample volume and $\langle m\rangle \equiv \langle M/M_\odot\rangle$ is the mean mass of the objects in solar masses. Note also that although the effects of the finite scale height of the Galaxy are not included, the mean distance of the computed samples ranges from $\sim$15 to 70 pc (sequences E and A, respectively, see below) and the maximum distance of any given star in *all* observationally selected samples is $\sim$240 pc. Thus, this omission will have little effect for most samples, since the local scale height is $\sim$250 pc.

For the velocity components, MCGoLF draws 3 times from the normal distribution,

$$v_i = G(v_{\rm rms}) , \tag{2}$$

where we have taken $\sigma = v_{\rm rms} = 40$ km s^{-1} for all three principal axes. There is no attempt to simulate a halo component to the velocity distribution, but this simple prescription reproduces the observed kinematics well enough for the purposes of this work.

Next is the discrimination based on the luminosity function. For this, MCGoLF makes use of a previously computed integrated LF (LFINT output) as the discriminator; this curve is normalized to a peak of unity on input, and spline interpolation coefficients are computed. For each trial, two uniform deviate random numbers are drawn. The first of these is scaled to provide a value for $\ell \equiv \log(L/L_\odot)$ between the maximum and minimum values for the sample,

$$\ell_{\rm test} = P(0, -8) , \tag{3}$$

where the minimum value is below the lowest luminosity where any objects would be expected, even in a 20 Gyr sample. The spline-interpolated value of the normalized LF at this random trial luminosity, $\Phi_{\rm LFINT}(\ell_{\rm test})$, is compared with the value of the second random number $\Phi_{\rm test}$. If $\Phi_{\rm test} < \Phi_{\rm LFINT}(\ell_{\rm test})$, i.e., if the test point is below the appropriate age curve, then the object "exists" in $V_{\rm samp}$ at the location (x_j, v_j, ℓ) and contributes to the overall space density $\Phi_{\rm true} = N_{\rm tot}/V_{\rm samp}$.

2.1.2. *The Observationally Selected Subsample and the $1/V_{\rm max}$ Luminosity Function Estimator*

At this point, we have a procedure for populating a region of space with objects that have luminosities drawn from a probability distribution function defined by integrated LFs of various ages. The next step is to determine whether the object makes it into the observationally selected subsample—i.e., whether the proper motion and V magnitude are within the specified observational limits. The proper motion is calculated from the relative space motion and distance, and objects are culled if the proper motion is below the input lower limit. For each object with $\mu \geq \mu_{\rm lim}$, we interpolate in the WDEC sequence data for a 0.6 $M_\odot$ DA WD model with thick surface layers to obtain $t_{\rm cool}$, $T_{\rm eff}$, and log g corresponding to $\ell_{\rm test}$, and then use these to interpolate in the atmospheric tables of Bergeron, Wesemael, & Beauchamp (1995) to obtain $M_{\rm V}$ and hence V magnitudes. If the V magnitude is brighter than the input limit, then the object becomes the ith member of the observationally selected subsample, and the data are stored ($\boldsymbol{r}_i$, $\boldsymbol{v}_i$, $v_{{\rm rad},i}$, $v_{{\rm tan},i}$, μ_i, ℓ_i, $T_{{\rm eff},i}$, and V_i). In our MC sample populations, roughly 200–600 objects exist in $V_{\rm samp}$ for each object in the observationally selected subsample.

Once the observationally selected subsample is populated, the luminosity function can be calculated. The classical estimator $\Phi = N/V$ for a volume-limited sample is of little practical use for analyzing the small-N, strongly localized and kinematically biased group of stars selected on the basis of proper motion and apparent magnitude. For these samples, the $1/V_{\rm max}$ method of Schmidt (1968, 1975) is generally regarded as the superior estimator of the luminosity function (Felton 1976). In this method, each star's contribution to the luminosity function is weighted by the inverse of the maximum volume in which this star would be observable. For example, for a given luminosity bin with index k, the space density is the sum (see Schmidt 1968)

$$\Phi_k = \sum_{i=1}^{N_k} \frac{1}{V_{{\rm max},i}} , \tag{4}$$

for the N_k objects with luminosities within the bin boundaries. For each object, $V_{{\rm max},i} = (4/3)\pi\beta r^3_{{\rm max},i}$, where here $\beta = \frac{1}{8}$, and

$$r_{{\rm max},i} = \min\left[r_i \frac{\mu_i}{\mu_{\rm lim}} , r_i 10^{-0.2(V_i - V_{\rm lim})} \right] , \tag{5}$$

is the maximum distance an object could have and still be within the observed limits in both apparent magnitude and proper motion. Following LDM, we set the uncertainty of each star's contribution equal to that star's contribution (e.g., 1 ± 1), and sum the errors in quadrature within a given luminosity bin,

$$\sigma_k = \left[\sum_{i=1}^{N_k} \left(\frac{1}{V_{{\rm max},i}} \right)^2 \right]^{1/2} . \tag{6}$$

One of the points we address below is how this arbitrary but conservative method of computing error estimates compares with the Monte Carlo simulation results.

3. RESULTS

3.1. *The Computational Grid*

In these simulations we draw from parent populations with kinematics similar to the observed population of white dwarf stars. For these preliminary calculations we have computed luminosity functions for sample populations differing only in their proper-motion limits. While we have varied the limiting magnitude limit in some runs, these runs provide no information beyond that presented below, since for these samples the selection is dominated by the proper-motion constraint. In a follow-up publication, we will present the results of our MC study of magnitude-limited surveys, such as that of Fleming, Liebert, & Green (1986). Because these samples penetrate considerably deeper—$D_{\rm max} \sim 1$ kpc—the calculations must include the scale height of the Galaxy as well as interstellar absorption.

Table 1 gives the parameter set grid for MC populations A–F. Note that population A is representative of the OSWH sample, and population E is representative of the LDM sample. For each input age (7–18 Gyr in increments of 1 Gyr) and chosen value of $N_{\rm obs}$, we draw $N_{\rm samp} = 10$ samples, and from these the luminosity functions are computed.

3.2. *Kinematics*

3.2.1. *Positions*

For samples selected as these have been—by proper motion and V magnitude—we would expect that the mean

TABLE 1

INPUT PARAMETERS FOR MONTE CARLO SIMULATION RUNS

Sequence	N_{obs}	t_{disk} (Gyr)	D_{max} (pc)	v_{rms} (km s^{-1})	μ_{lim} (arcsec yr^{-1})	V_{lim} (mag)
A	50, 200	7(1)18	400	40	0.15	19
B	50, 200	7(1)18	300	40	0.20	19
C	50, 200	7(1)18	150	40	0.40	19
D	50, 200	7(1)18	100	40	0.60	19
E	50, 200	7(1)18	100	40	0.80	19
F	50, 200	7(1)18	100	40	1.00	19

distance would be small and that the sample would be biased against objects with small space velocities. Both of these expectations are realized in these simulations. Figures 2 and 3 show the positions and relative luminosities of the 50 objects that comprise two representative, 10 Gyr old samples drawn from populations A′ and E′,[1] respectively, where glyph size is proportional to ℓ, and the scale is the same in both figures. In addition, we show the positions (as points) of all the $N_{tot} - N_{samp}$ objects in V_{samp} that did not satisfy the selection criteria. Figure 2 shows a $D_{max} = 200$ pc volume and indicates also the relative size of the $D_{max} = 50$ pc volume of Figure 3. Both samples are populated uniformly, but the observationally selected subsamples are strongly biased toward $r = 0$.

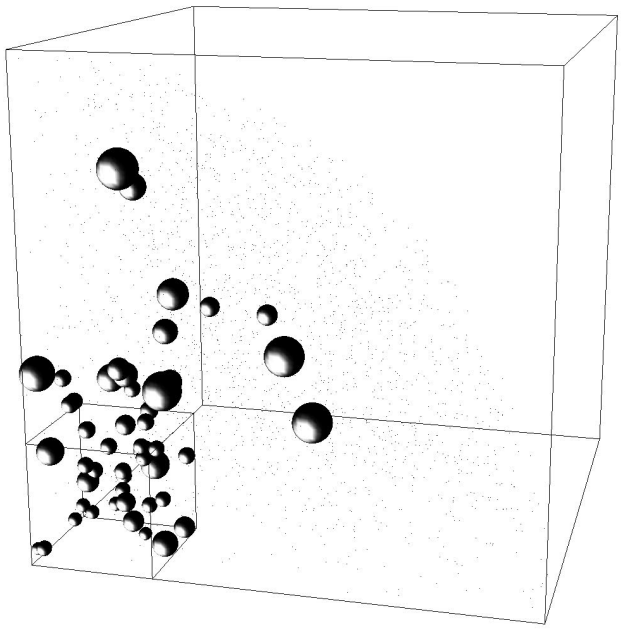

FIG. 2.—Positions and relative luminosities of the 50 "observationally selected" objects drawn using population sample A′ and an age of 10 Gyr, which approximates that of OSWH. Sample objects are shown as glyphs; positions of rejected objects that exist in V_{samp} are shown as points. The bounding box has volume (200 pc)^3. The relative sizes of the glyphs indicate the luminosity ℓ—bigger is brighter. The inset box shows the (50 pc)^3 volume of Fig. 3, showing similar data for population sample E′. The scale relating ℓ to glyph size is the same for the two figures. Clearly, the lower proper-motion limit of A′ results in a much larger effective sample volume. As a result, brighter objects, which are intrinsically rare, have a greater chance of being included in the observationally selected sample.

[1] We designate these particular sample populations A′ and E′ since their D_{max} values differ from those given in Table 1 (here $D_{max} = 200$ and 50 pc, respectively, for A′ and E′), while all other parameters are the same. For the purpose of these figures and the accompanying discussion, it is desirable to set D_{max} to the *typical* maximum distance obtained in the samples, instead of choosing it to be well beyond the maximum distance at which a star could be and still make it into the observationally selected subsample, as is the case for the results discussed in the remainder of this work.

The figures also clearly demonstrate the expected effect of the lower proper-motion limit sampling a significantly larger volume. If proper motion alone was the selection criterion, then we would expect that population A would sample a volume $(0.15/0.8)^{-3} \approx 150$ times that of sample E. We find that to acquire 50 objects in each of the two "observed" subsamples of A′ and E′ ($t_{disk} = 10$ Gyr, $D_{max} = 200$ pc), an average total of $\sim$1560 objects must populate V_{samp} for parameter set A′ and $\sim$85,300 for E′—a ratio of 55.

Figure 4 shows the radial distributions of the 500 point samples we have for each age, for populations A, C, and E, and demonstrates the sensitivity to proper-motion limit μ_{lim}. Also shown to guide the eye is a dotted line at the average distance of each observed sample population, 65.8, 30.3, and 16.2 pc, respectively. The ratio $(65.8/16.2)^3 \approx 67$ gives a measure of the ratio of the effective sampling volumes of population A relative to population E, which is complementary to and consistent with the estimate above. A final, extreme measure is given by the cube of the ratio of the *maximum* distances for stars in the observationally selected subsamples, $(230.9/48.0)^3 \approx 110$. This is closer to the

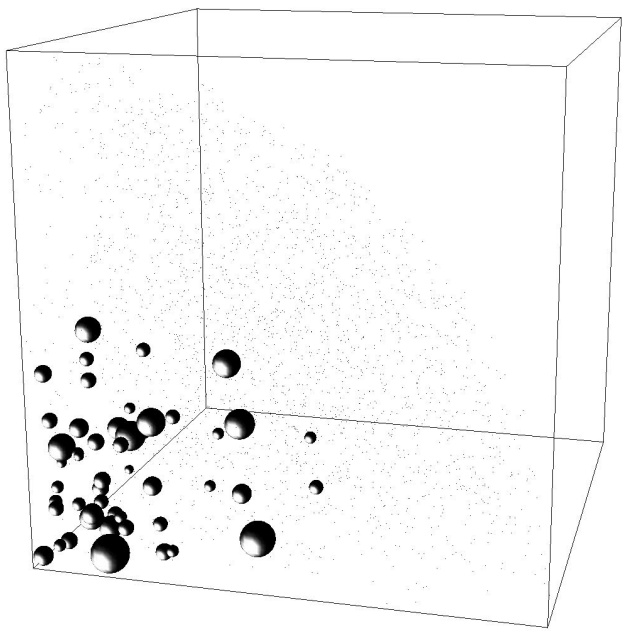

FIG. 3.—Same as Fig. 2, but for a 50 object draw from population sample E′, which approximates that of LDM. Here, the bounding box has volume (50 pc)^3.

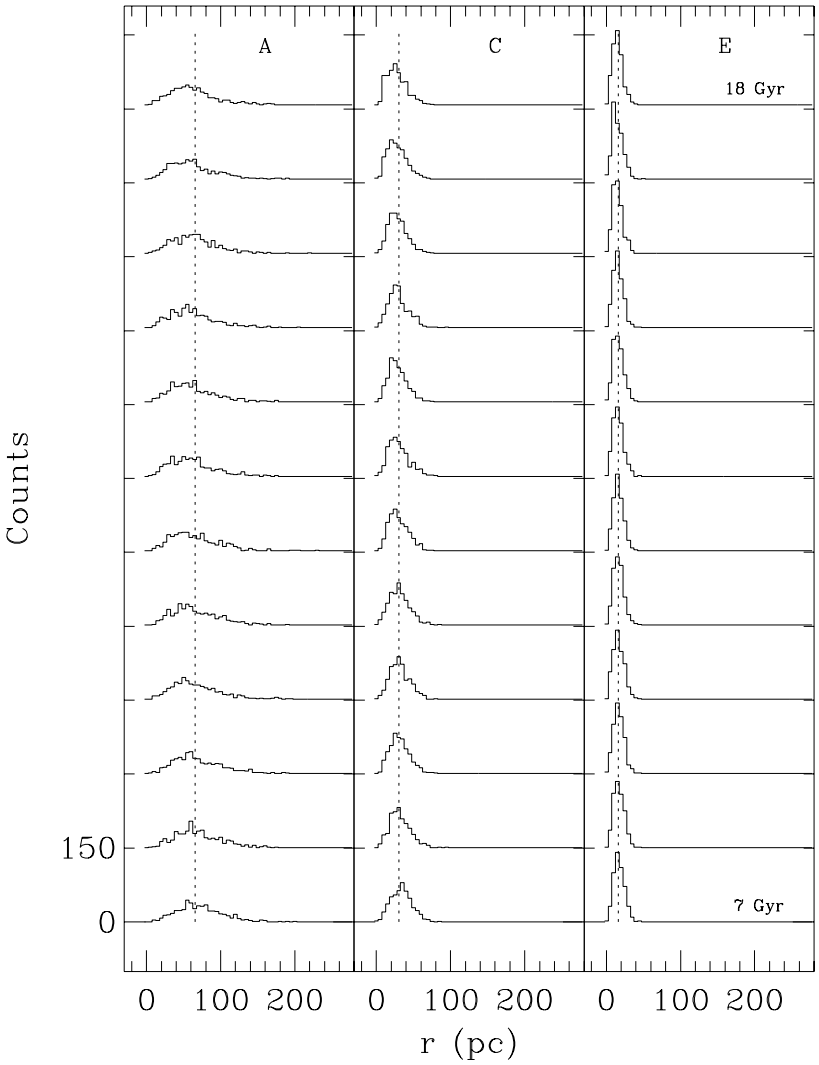

FIG. 4.—Histograms showing radial distributions as a function of age for populations A, C, and E. The dotted lines indicate the average distance of each sample population: 65.8, 30.3, and 16.2 pc, respectively, for sample populations A, C, and E. The samples cluster progressively closer to the origin for larger proper-motion limits, as expected.

value of ~ 150 expected if proper motion were the only selection criterion. Thus, population A samples an effective volume ~ 60–100 times larger than E, supporting OSWH's claim that their luminosity function samples a volume at least 50 times larger than that of LDM.

Comparing populations C and E, the cube of the ratio of mean distances, $(30.3/16.2)^3 = 6.5$, is very near the value of $(0.4/0.8)^{-3} = 8.0$ expected if the samples were selected only by proper motion. A final, subtle but expected effect apparent in Figure 4 is that older samples cluster progressively nearer the origin as the number of very faint objects in these fixed-number samples increases.

The fact that the ratio of effective sample volumes is near the ratio expected for selection by proper motion only suggests that stars are culled most frequently by proper motion, and only rarely because they are too faint in V. The results presented in Table 2, which summarizes the simulation selection statistics for populations A′ and E′, confirm these suspicions. We find, for population E′, that of the 13,702 objects culled to arrive at a final observed sample of 500, fully 86% were brighter than $V_{\rm lim}$ but had $\mu < \mu_{\rm lim}$, whereas only 0.04% were fainter than $V_{\rm lim}$ but passed the proper-motion test. The remainder failed both tests. The statistics for population A′ are more balanced: 13% are culled by proper motion only, 5% by V magnitude only, and the remainder fail both tests.

We can view these results in graphical form using a plot of the logarithm of the cumulative count versus logarithm

TABLE 2

SELECTION STATISTICS

SEQUENCE	$N_{\rm obs}$	$\mu_{\rm lim}$ (arcsec yr^{-1})	$D_{\rm max}$ (pc)	$N_{\rm tot}$	NUMBER REJECTED BY		
					μ	V	Both μ and V
A′	500	0.15	200	15,580	1891	788	12401
E′	500	0.80	50	14,202	11778	6	1918

of proper motion μ_0, where the cumulative count is defined as

$$C(\mu_0) \equiv \log \sum_{\mu > \mu_0} n \, . \tag{7}$$

If the sample is complete, then the relation $C(\mu_0)$ versus log μ_0 will have a slope of -3 (e.g., Oswalt & Smith 1995). Figure 5 shows the cumulative counts for 2000 point samples drawn from populations A–E. Also shown for comparison are lines with slopes of -3. Our ideal observational selection (i.e., zero observational bias/error) results in samples that are complete down to proper-motion limits of $\mu_{\rm lim} \approx 0\farcs4$ yr^{-1}, as indicated by the -3 slopes obtained from populations C, D, and E. Populations A and B, however, show deficits near their proper-motion limits, indicating that a significant fraction of these objects are being culled by V magnitude.

Observationally, it is no simple matter to insure that WD surveys are complete, yet we can reliably estimate the space density only when the observational limits are chosen so that completeness is either known (assumed) to be 100% or the fractional incompleteness can be quantitatively estimated. Indeed, LDM chose their lower proper-motion survey limit of $\mu_{\rm lim} = 0\farcs8$ yr^{-1} in an attempt to make their observational database complete. The Luyten and Giclas catalogs of proper-motion objects are complete down to a limit of $\sim 1\farcs0$ yr^{-1} and include stars with μ as small as $\mu \geq 0\farcs1$ yr^{-1}. Oswalt & Smith (1995) find that the cumulative count diagrams of these survey data, while log-linear, indicate significant incompleteness, in that the slopes are significantly different from -3. Below $\sim 1\farcs0$ yr^{-1}, the data indicate progressive incompleteness and hence are not immediately useful. OSWH employed a completeness correction procedure that made use of the relative slopes of the cumulative count plots to effectively account for that fraction of objects that a proper-motion survey misses. A summary of this procedure was presented in OSWH; details will be presented elsewhere. The raw and corrected curves shown in OSWH are roughly parallel, suggesting that the incompleteness is not a strong function of $M_{\rm V}$, although it is a function of apparent magnitude. In the next paper in this series, we plan to explore more fully the consequences of photometric uncertainties and survey incompleteness on the derived observational LF.

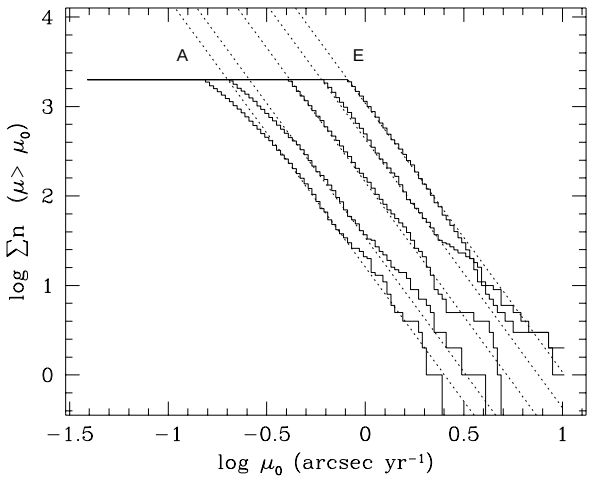

FIG. 5.—Cumulative counts of the number of objects with proper motion greater than the abscissa value for 2000 object samples drawn from populations A–E. Also shown for comparison are dotted lines with slopes of -3, which are indicative of complete samples. Note that the samples from populations C, D, and E are complete, but that populations A and B show deficits near their proper-motion limits. This indicates that the former are culled almost entirely by proper motion, whereas some non-negligible fraction of the latter are culled by apparent magnitude.

The standard method of checking for completeness in the $1/V_{\rm max}$ technique is to compute $\langle V/V_{\rm max} \rangle$ for the sample. For complete samples, $\langle V/V_{\rm max} \rangle = 0.50$. Both the OSWH and LDM samples are incomplete based ontheir $\langle V/V_{\rm max} \rangle$ values of 0.324 ± 0.046 and 0.369 ± 0.046, respectively. Our MC simulations are complete, with $\langle V/V_{\rm max} \rangle = 0.50$ to within the errors.

Our MC simulations provide an ideal test bed to explore the reliability of the space density estimation in Schmidt's $1/V_{\rm max}$ method. For each sample we calculated $\Phi_{V_{\rm max}}$ (see eq. [8]) and then compared this with $\Phi_{\rm true}$. In Figure 6 we show the histograms of the number of samples as a function of $R \equiv \Phi_{V_{\rm max}}/\Phi_{\rm true}$ for populations A–E, and for 50 point and 200 point samples. The data comprising each panel within the figure come from the 10 samples for each of the 12 ages, 7–18 Gyr, inclusive. Some panels do not show all the data; the number of samples beyond the right edge of these panels is indicated in the lower, right-hand corner.

It is clear from this figure that the $1/V_{\rm max}$ technique provides a reliable estimate of the space density.[2] The distributions are skewed, however. For the 50 point samples, we find a global mean $\langle R \rangle = 0.97 \pm 0.49$ and a median of $R_{\rm med} = 0.88$, whereas the 200 point samples yield $\langle R \rangle = 0.98 \pm 0.24$ and $R_{\rm med} = 0.93$. The width of the 50 point distributions suggests that the factor of 2 difference between the LDM and OSWH space densities could simply be the result of sampling statistics within the $1/V_{\rm max}$ method. An additional contributing factor may be that the LDM data were incomplete but not corrected for incompleteness as were the OSWH data.

3.2.2. *Velocities*

Figure 7 shows the velocity distributions of 2000 point, 10 Gyr samples from populations A and E. These distributions are similar to that obtained by Sion et al. (1988, their Fig. 1) in a study of WD kinematics, as expected since we used the Sion et al. results to set our $v_{\rm rms}$ value and velocity distribution width. The primary difference between the observed and simulated data is the deficit of low- and high-velocity objects in the simulated data: the former results from a higher proper-motion limit, and the latter results from the halo and thick-disk population stars in the observed sample. As expected, the velocity distribution for population E is biased toward higher velocities compared to that of population A. In addition, there is a very weak trend for the oldest samples to have mean $v_{\rm tan}$ smaller than for the youngest samples from a given population. This is simply a result of the oldest samples' smaller mean distances.

3.3. *White Dwarf Luminosity Function Turndown Ages: Statistical Uncertainties*

In Figures 8–11, we show the results for parameter set A for input ages of 7, 10, 13, and 16 Gyr. For comparison, the input LFINT curves are also shown for these ages, and to facilitate comparison of the Monte Carlo results with the

[2] Because of a coding error in an early version of MCGoLF, a trend in $\Phi_{V_{\rm max}}/\Phi_{\rm true}$ vs. proper motion was erroneously reported in Wood (1997).

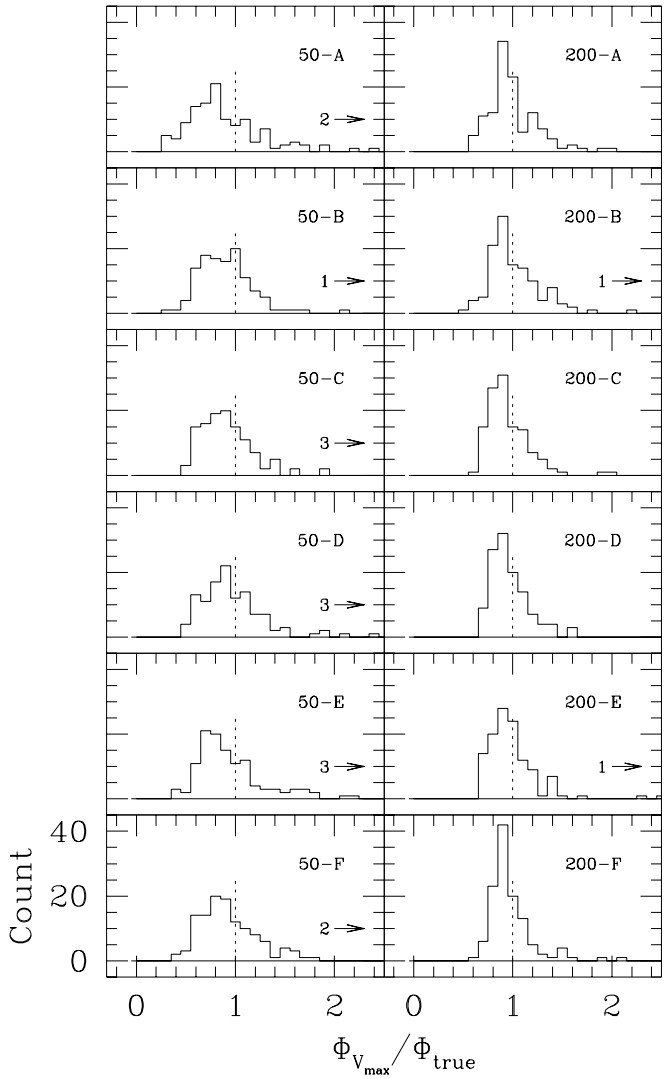

FIG. 6.—Panel plot showing the histogram distributions of the ratio $\Phi_{V_{max}}/\Phi_{true}$ as a function of proper-motion limit for both 50 object and 200 object samples. Each panel shows the histogram of the 120 $\Phi_{V_{max}}/\Phi_{true}$ values resulting from the 10 samples at each of the 12 input ages (7–18 Gyr, inclusive). The number of points that fall outside the plot bounds—if nonzero—are indicated in the lower, right-hand corner of each panel. We find no significant trend as a function of proper-motion limit. The median $\Phi_{V_{max}}/\Phi_{true}$ is 0.91 and the mean is 0.97, suggesting that observed space densities from "complete" samples could in principle be corrected upward by $\sim$10%, although this is not something we would recommend, since the uncertainty in Φ is significantly larger than this. Note that we also searched for a trend in $\Phi_{V_{max}}/\Phi_{true}$ as a function of age and found none.

input LF, the former have been renormalized to the latter (but see below). Within each panel, there are 10 independent distributions drawn from the parent population. Each distribution is binned twice, with their respective bin centers differing by $\frac{1}{2}$ the bin width (i.e., the "a" and "b" LFs in the figures); the ordinate scale is correct for the bottom ("1a" and "1b") distribution, and the other curves have been successively offset by a constant. The number of objects contributing to each bin is indicated above each point, and the errors have been computed according to equation (6) above. For bins populated by a single object, the formal uncertainty is unbounded in the negative direction, but to avoid visual confusion we have shown these as error bars with a length of 2.0 (the separation between the curves is

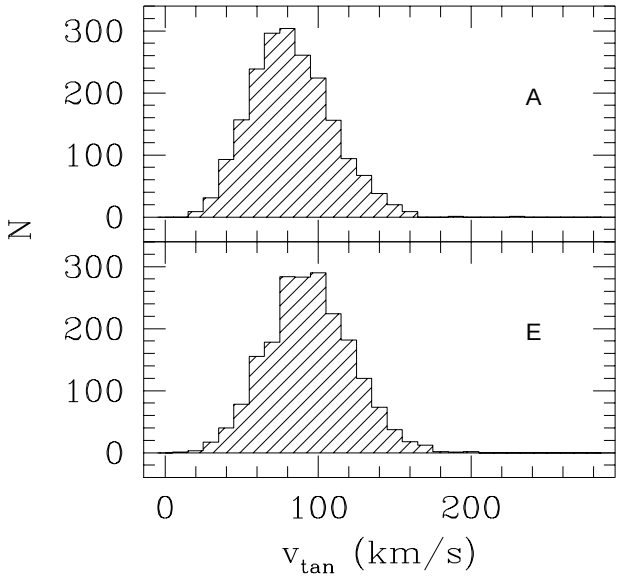

FIG. 7.—Histograms of tangential velocity for 10 Gyr samples from populations A and E. The distributions are similar to observed distributions but lack the low- and high-velocity tails (see text).

3.0). Next to each pair of curves are three numbers. The top one is the sample number, the middle one is the summed $1/V_{max}$ space density,

$$\Phi_{V_{max}} = \sum_{i=1}^{N_{obs}} \left(\frac{1}{V_{max,i}} \right), \tag{8}$$

and the bottom one is the true space density,

$$\Phi_{true} = N_{tot}/V_{samp}\ , \tag{9}$$

where the space densities expressed in units of $(10^3\ pc^3)^{-1}$. Note that although $\Phi_{V_{max}}$ can differ from Φ_{true} by a factor of 2 or more, the overall *shape* of the observationally selected sample LF does not differ in any systematic way from the input LFINT curves. This is an important result because it means that we can still derive reliable age estimates from samples with proper-motion limits well below the 0.″4 yr^{-1} "complete" sample limit discussed above. Adopting a lower proper-motion limit for the survey results in an enormous increase in the number of objects that can contribute to the LF, with a corresponding increase in the accuracy of the age determination.

The 7 Gyr samples would all be assigned ages within 0.5 Gyr of the input age, but any attempts to infer variations in the recent star formation rate from the LF points with $\ell \gtrsim -3.5$ ($t_{cool} \lesssim 2$ Gyr) would be futile. An examination of the other panel LF plots shows this is a general result for samples selected by both proper motion and apparent magnitude. The 10 Gyr samples show considerably more variation in the location of the lowest luminosity bin: three of the 10 samples would be interpreted as having ages 1–2 Gyr different from the input age, and two of the 10 have peak LF bins that are $\sim 2\,\sigma$ below the input peak. The 13 and 16 Gyr samples also show considerable variation in the lowest luminosity bins, and in $\sim$30% of the samples the inferred age would be 1–2 Gyr ($\sim$15%) off the input age. The most dramatic result from the 16 Gyr sample, however, is that the extra 3 Gyr adds only about three additional stars to the log $(L/L_\odot) = -5$ and fainter bins in these 50 point samples.

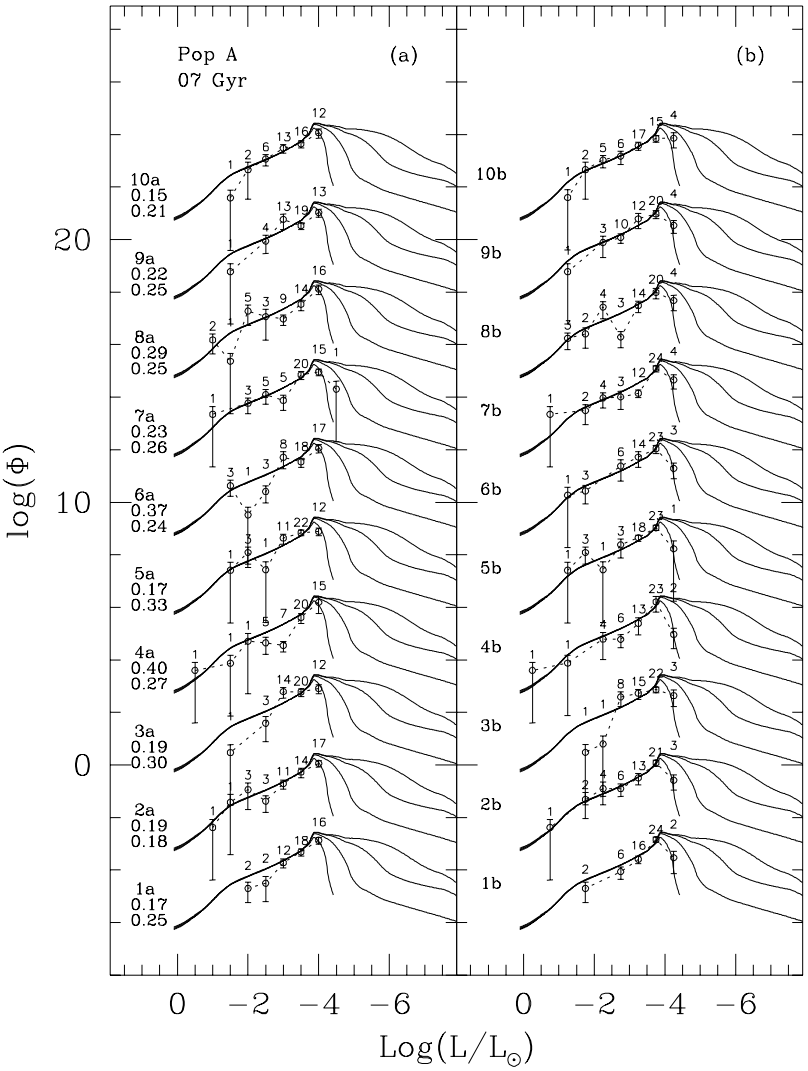

FIG. 8.—MCGoLF results for 10 samples drawn from the parent population specified by the sequence A parameters in Table 1 for an age of 7 Gyr. The bottom curve has approximately the proper normalization for the space density, and the other curves have been successively offset by 3.0 dex. The left and right LFs reflect two different binnings of the same data—the two distributions are offset by 1/2 the bin width. Underneath the left-hand labels are the $\Phi_{V_{max}}$ and Φ_{true} space densities for the sample in units of 10^3 pc^3. Error bars indicate 1 σ errors calculated as discussed in the text with the exception of bins that have only one member; these formally would have error bars of $+0.3$ and $-\infty$, but for purposes of display we set $-\infty \rightarrow -2$. Also included for purposes of comparison are the integrated LF curves for disk ages 7, 10, 13, and 16 Gyr. For clarity, the 7 Gyr curve has been truncated at the cool end (cf. Fig. 1). Note the sample-to-sample variations in the bright end of the LF—these results suggest that variations in the recent star formation rates cannot be reliably inferred from the bright end of the LF if derived using the $1/V_{max}$ estimator.

This suggests that our leverage on the local age is rather weak beyond an age of 13 Gyr, and so significantly larger observational samples are needed. The bright end of these sample population A LFs again show considerable variations relative to the input curve in roughly half of the samples, and these variations become more extreme for the older samples.

Figure 12 shows the 10 Gyr samples from population E. Because population E samples a much smaller volume than population A and the space density of bright objects is intrinsically low, these LFs are biased toward fainter luminosities, as expected. The statistical variations in the LFs are again substantial. Indeed, based on these noise-free simulations, it is perhaps surprising that the observed LFs are as smooth as they are. In any event, these simulations taken in toto demonstrate that no conclusions regarding the recent star formation rate can be drawn from samples selected on the basis of proper motion alone. The Fleming et al. (1986) LF of hot white dwarfs, used by LDM, is a magnitude-limited sample only (not magnitude and proper motion) and so may not necessarily be subject to these same uncertainties, but caution is probably warranted when interpreting fine details of any WDLF. We will use our MC code to explore the statistical variations in magnitude-limited samples in a future publication.

Figure 13 shows 10 200 point samples for an age of 10 Gyr. Here, we see that only one sample (sample 6) could be interpreted to have an age ~ 1 Gyr different from the input age; the others are all within ~ 0.5 Gyr of the input age. The 7, 13, and 16 Gyr samples (not shown) also support these conclusions. As above, the largest variations in the inferred ages results from samples with $N \lesssim 5$ objects in the faintest bin. Rebinning the 200 point samples into bins with a width of 0.25 dex does not significantly improve the scatter at the faint end, since this results in several bins with $N \lesssim 5$. These results, however, suggest that observed samples with $N \gtrsim$

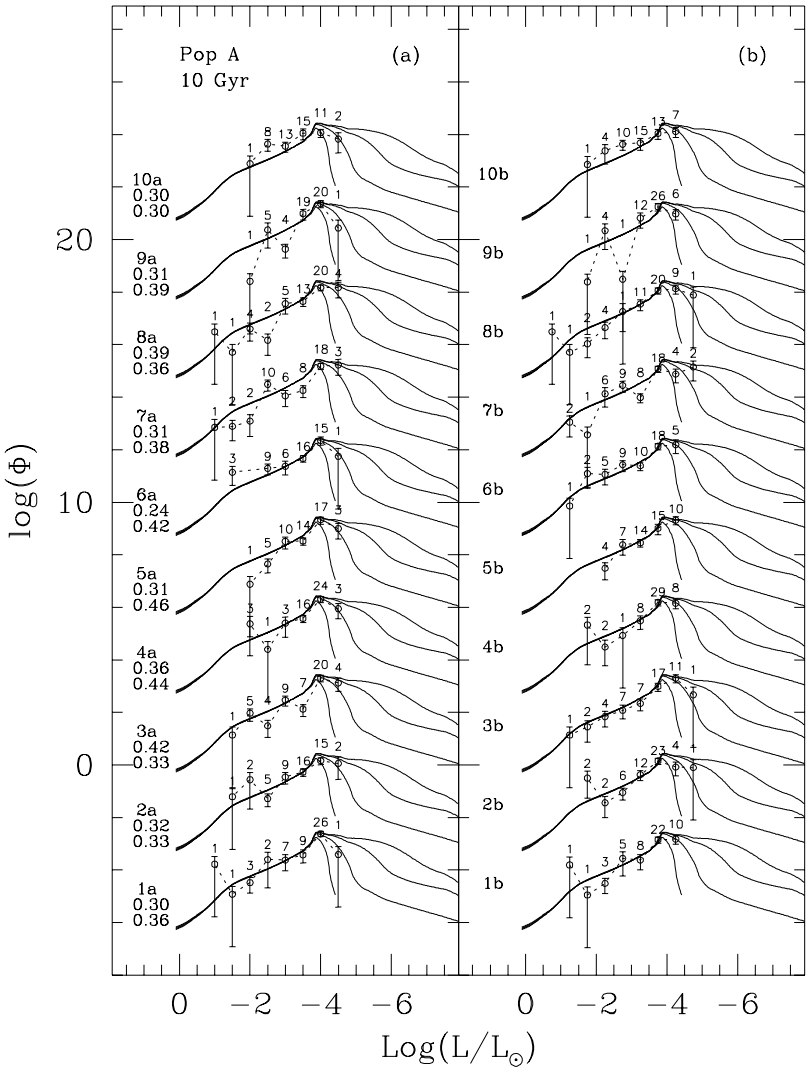

FIG. 9.—Same as Fig. 8, but for an age of 10 Gyr. Note in this and the following two figures that roughly 30% of the samples would give estimated ages 1–2 Gyr different from the input age.

200 stars should yield uncertainties in the age estimates that are at the $\sim 5\%$ level, and such samples are currently being analyzed (Smith 1997).

4. DISCUSSION

The white dwarf luminosity function has been used extensively in recent years as a probe of the age and star formation history of the solar neighborhood in the Galaxy. The goal of this work has been to investigate the inherent statistical uncertainties in the recent determinations of the white dwarf luminosity function by means of extensive Monte Carlo simulations. We find that Schmidt's $1/V_{\rm max}$ estimator provides an extremely useful but imperfect probe of the white dwarf luminosity function. Three major results have emerged from this study.

First, the space densities obtained using the $1/V_{\rm max}$ technique provide robust estimates of the true local space density. Sample-to-sample variations in these noise-free data suggest an intrinsic statistical uncertainty of roughly 50% and 25% for 50 and 200 point samples, respectively.

Second, ages inferred from observed distributions must be considered uncertain by $\sim 15\%$ from sampling statistics alone if there are ~ 50 objects in the sample and $N \lesssim 5$ objects in the lowest luminosity bin. For samples with $N \approx 200$ objects, the uncertainties are typically $\lesssim 10\%$. These results are consistent with the conservative error estimates adopted by LDM and OSWH (see eq. [6]). Note that while other cooling codes yield differing estimates for cooling timescales, it seems likely to us that the internal uncertainties will remain at the 10%–15% level. Both LDM and OSWH have three objects in their lowest luminosity bins, so it is possible, but unlikely with a $\lesssim 10\%$ probability that these two samples are consistent with a single parent population. Indeed, these results suggest that it may be best to *choose* the bin centers such the bin widths are as narrow as possible while still leaving the lowest luminosity bin with $N \gtrsim 5$ objects, although the trade-off is that this would move the lowest luminosity bin to higher luminosity and hence reduce the leverage on the age determination. It is possible that a statistical test (e.g., Kolmogorov-Smirnov) on a nonbinned sample of the coolest objects would prove to be a superior tool for the analysis of the WDLF (G. Chabrier 1997, private communication).

Third, even the larger samples have LFs whose bright ends show substantial deviations from the input functions,

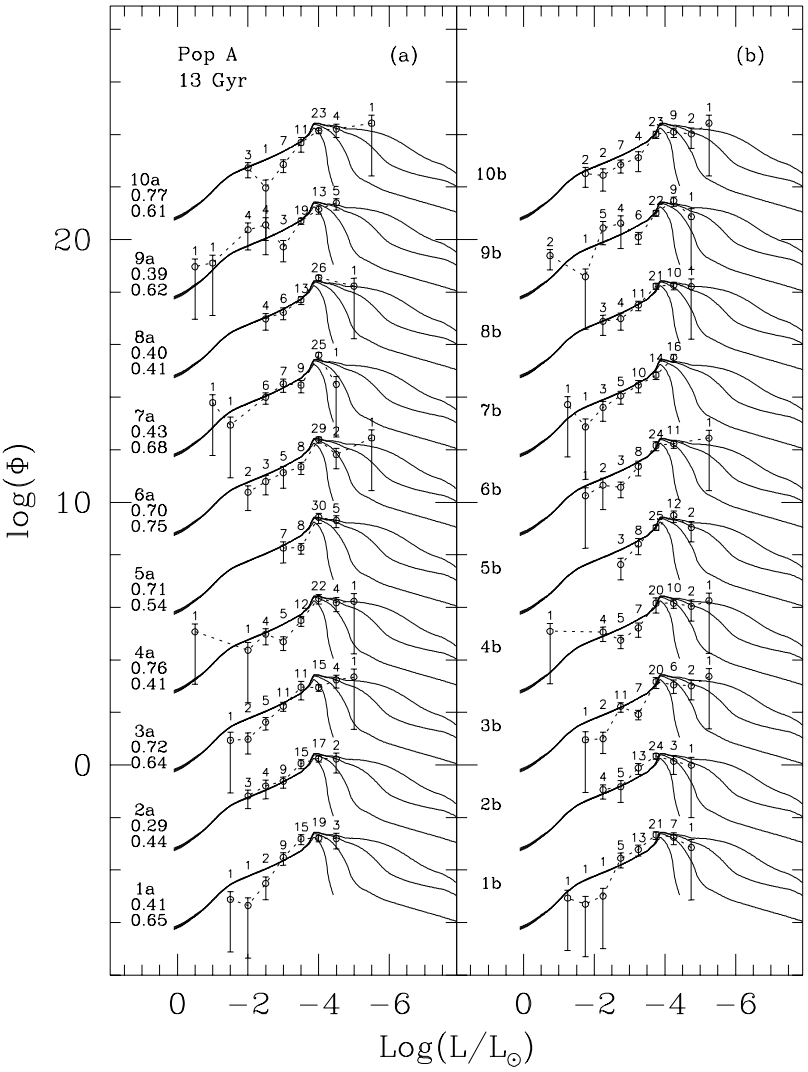

FIG. 10.—Same as Fig. 8, but for an age of 13 Gyr

suggesting that it is impossible to reliably infer any *variations* in the recent star formation rate based on samples selected by both proper motion and apparent magnitude.

Assuming a 1 Gyr uncertainty from sampling statistics and adding this to the $\sim$1 Gyr uncertainty resulting from an incomplete understanding of the detailed inputs to white dwarf and galactic evolution models (Wood 1992), white dwarf cosmochronology can currently be considered to give ages good to roughly $\pm$20%. With larger observational samples that will soon be available (Smith 1997), and with continuing improvements in the determinations of white dwarf composition profiles and constitutive physics in the evolutionary models, this uncertainty should be reduced to less than $\pm$10% in the near future.

Our thanks to Don Winget and Steve Kawaler for useful discussions and to Nathan Miller for creating the *IBM Data Explorer* networks used to visualize the data in Figures 2 and 3. Our sincere thanks to the referee, Gilles Chabrier, for pointing out an error in the original manuscript. This work was supported in part by the National Science Foundation through grants AST 92-17988 (M. A. W.) and AST 90-16284 (T. D. O.) and the NASA Astrophysics Theory Program through grant NAG 5-3103 (M. A. W.). Additional support was provided to Nathan Miller by the NSF through the SARA Research Experiences for Undergraduates Summer Internship Program (NSF AST 94-23922).

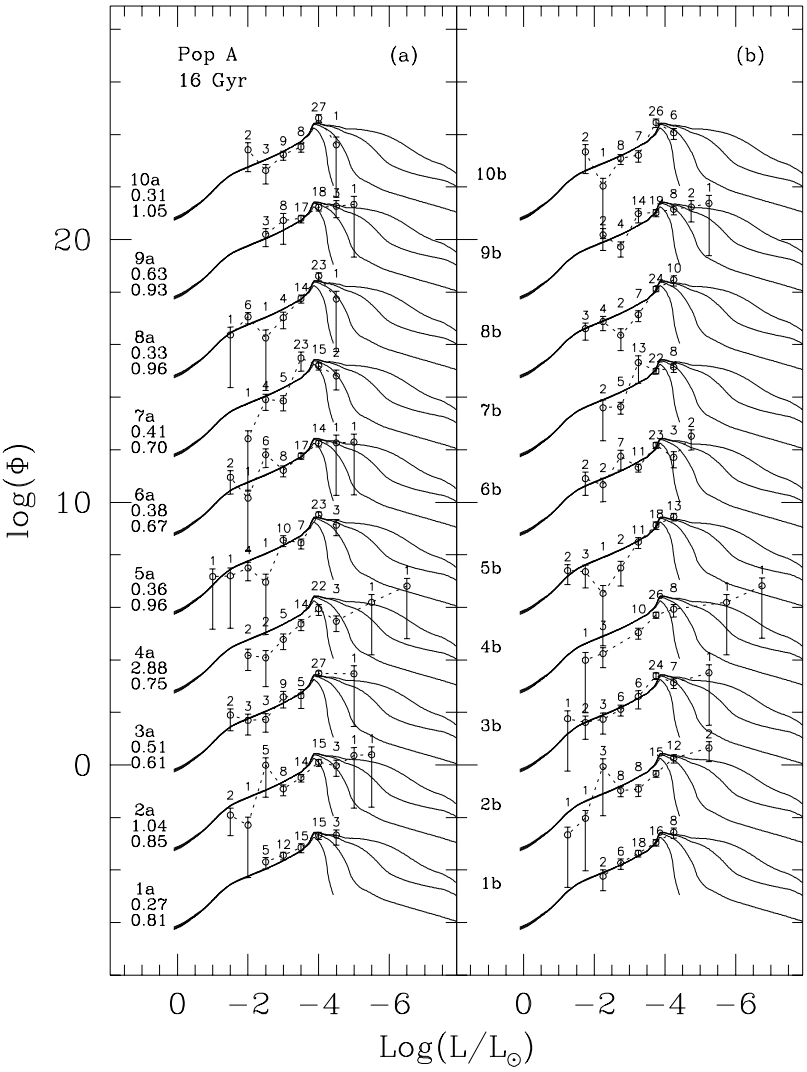

FIG. 11.—Same as Fig. 8, but for an age of 16 Gyr

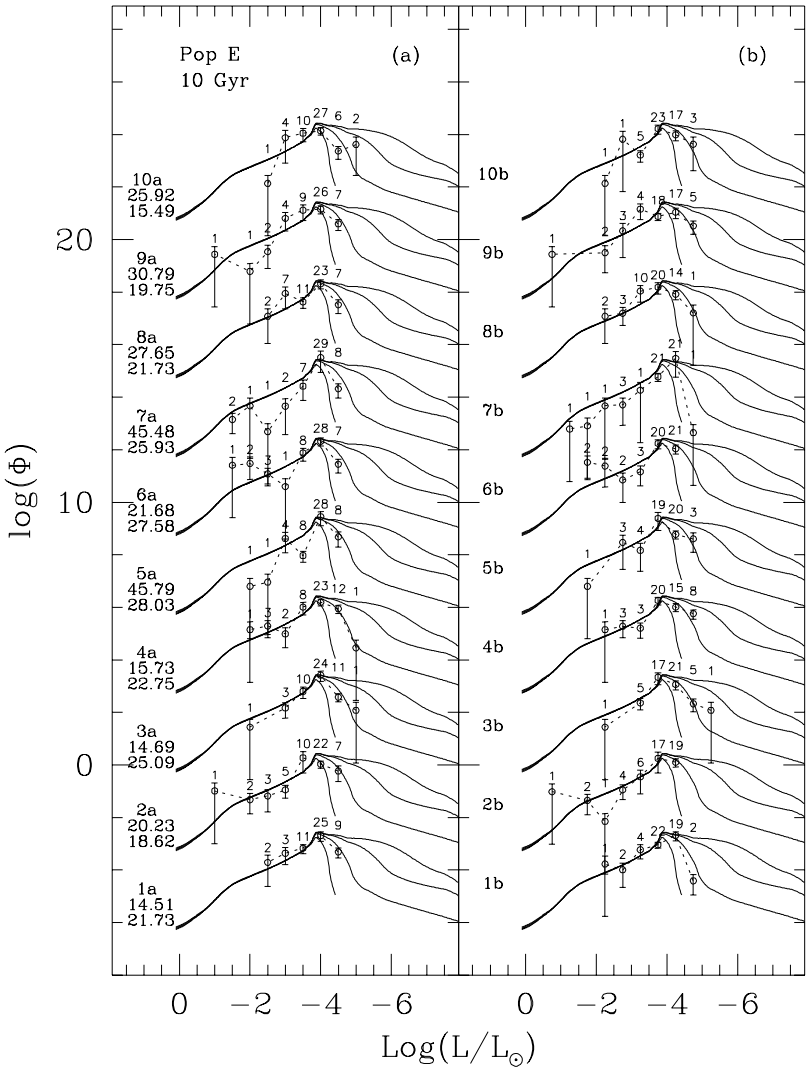

FIG. 12.—Same as Fig. 9, but for parameter set E. Compare the statistical noise in this figure with that of Figs. 1 and 9.

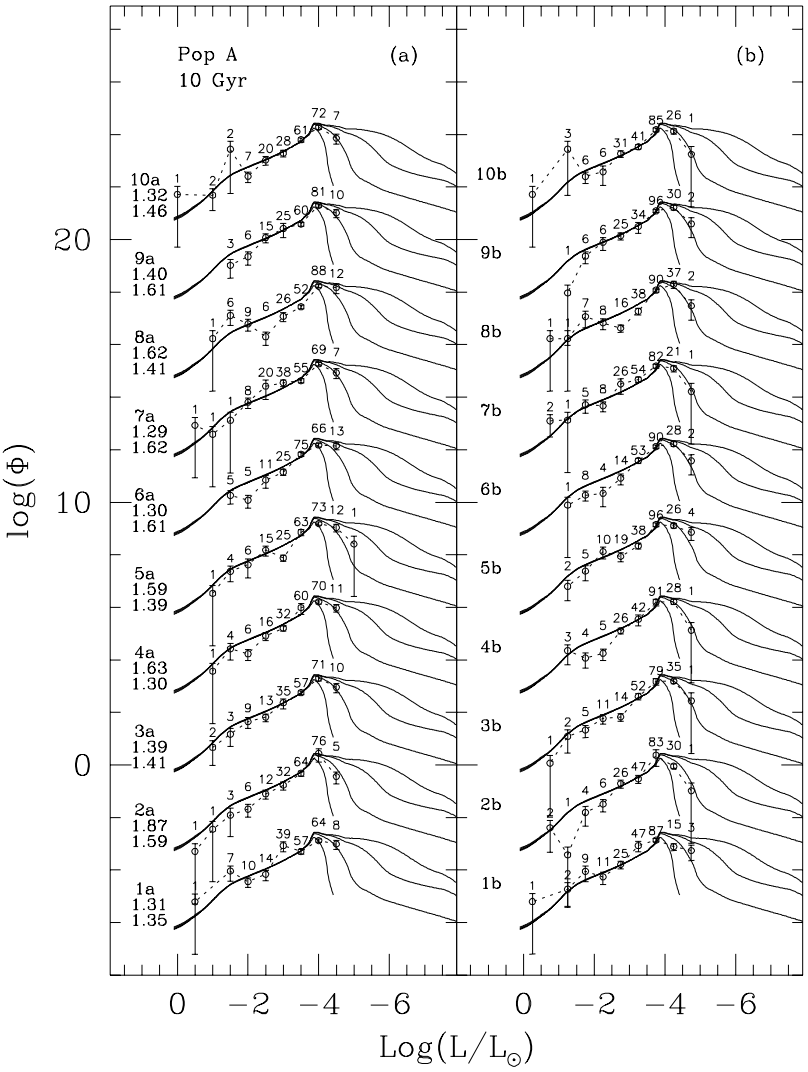

FIG. 13.—Same as Fig. 9, but for 200 point samples and an age of 10 Gyr. In this figure, the ages of all samples would be assigned ages within 0.5 Gyr of the input age, but as seen before, statistical variations at the bright end of the LF make derivations of the recent star formation rate meaningless.

REFERENCES

Bergeron, P., Wesemael, F., & Beauchamp, A. 1995, PASP, 107, 1047
Bolte, M., & Hogan, C. J. 1995, Nature, 376, 399
Burkert, A., Truran, J. W., & Hensler, G. 1992, ApJ, 391, 651
Carney, B. W., Latham, D. W., & Laird, J. B. 1990, AJ, 99, 572
Chaboyer, B. 1995, ApJ, 444, L9
Chiappini, C., Matteucci, F., & Gratton, R. 1997, ApJ, 477, 765
D'Antona, F., & Mazzitelli, I. 1978, A&A, 66, 453
Felton, J. E. 1976, ApJ, 207, 700
Fleming, T. A., Liebert, J., & Green, R. F. 1986, ApJ, 308, 176
García-Berro, E., Hernanz, M., Mochkovitch, R., & Isern, J. 1988, A&A, 193, 141
Hernanz, M., García-Berro, E., Isern, J., Mochkovitch, R., Segretain, L., & Chabrier, G. 1994, ApJ, 434, 652
Iben, I., Jr., & Laughlin, G. 1989, ApJ, 341, 312
Koester, D., & Chanmugam, G. 1990, Rep. Prog. Physics, 53, 837
Lamb, D. Q., & Van Horn, H. M. 1975, ApJ, 200, 306
Liebert, J., Dahn, C. C., & Monet, D. G. 1988, ApJ, 332, 891 (LDM)
———. 1989, in IAU Colloq. 114, White Dwarfs, ed. G. Wegner (Berlin: Springer), 15
Marsaglia, G. 1987, Florida State University Report FSU-SCRI-87-50
Mestel, L. 1952, MNRAS, 112, 583
Noh, H.-R., & Scalo, J. 1990, ApJ, 352, 605
Oswalt, T. D., & Smith, J. A. 1995, in White Dwarfs, ed. D. Koester & K. Werner (Berlin: Springer), 24
Oswalt, T. D., Smith, J. A., Wood, M. A., & Hintzen, P. M. 1996, Nature, 382, 692
Press, W. H., Flannery, B. P., Teukolsky, S. A., & Vetterling, W. T. 1986, Numerical Recipes (Cambridge: Cambridge Univ. Press)
Schmidt, M. 1959, ApJ, 129, 243
———. 1968, ApJ, 151, 393
———. 1975, ApJ, 202, 22
Segretain, L., Chabrier, G., Hernanz, M., Garcí-Berro, E., Isern, J., & Mochkovitch, R. 1994, ApJ, 434, 641
Sion, E. M., Fritz, M. L., McMullin, J. P., & Lallo, M. D. 1988, AJ, 96, 251
Smith, J. A. 1997, Ph.D. thesis, Florida Institute of Technology
Winget, D. E., Hansen, C. J., Liebert, J., Van Horn, H. M., Fontaine, G., Nather, R. E., Kepler, S. O., & Lamb, D. Q. 1987, ApJ, 315, L77
Wood, M. A. 1990, Ph.D. thesis, Univ. Texas at Austin
———. 1992, ApJ, 386, 539
———. 1995, in White Dwarfs, ed. D. Koester & K. Werner (Berlin: Springer), 41
———. 1997, in White Dwarfs, ed. J. Isern, M. Hernanz, & E. Garcia-Berro (Dordrecht: Kluwer), 105
Yuan, J. W. 1989, A&A, 224, 108
———. 1992, A&A, 261, 105